

The Optical properties of Fe-Doped TiO₂ films prepared by Hydrothermal Technique

Sattar J. Hashim*, Odai N. Salman and Khaleel I. Hasson

Department of Applied Sciences, University of Technology, Baghdad, Iraq

Articles Information

Received:
19.01.2020
Accepted:
31.08.2020
Published:
26.09.2020

Keywords:

Titanium dioxide Fe doping
Hydrothermal deposition
Optical properties

DOI: 10.22401/ANJS.23.3.02

*Corresponding author: sattarjabir314@gmail.com

Abstract

TiO₂ films doped with Fe at (0.1, 0.3, 0.7, 1.5 at %) were successfully deposited on the fluorine doped tin oxide (FTO)-glass substrate using hydrothermal technique. X-Ray Diffraction (XRD) analysis showed that the only phase obtained of TiO₂ is rutile. Moreover, the crystallinity did not have remarkable change after doping. Ultra violet-visible (UV-vis) spectroscopy analysis show that the energy band gap value (E_g) decreases slightly with the increase of the doping concentration from 0.1 to 0.3 at%. The reflectivity measurements in general gave identical results but with higher values of E_g. Urbach energy for doping concentrations 0.7 and 1.5 at % is quite high and in the range 1-2 eV.

1. Introduction

Titanium dioxide (TiO₂) films attracted high attention in the last decades because of its easy manufacture, low cost, nontoxicity and its promising applications in third generation solar cells [1-2]. As a material, TiO₂ has unique chemical, physical, and optical characteristics such as a wide and direct bandgap, good photocatalytic activity, photostability, chemical stability, high melting point, and high refractive index [3-7].

The main forms of TiO₂ crystalline are anatase (A), brookite (B), and rutile (R) [8]. Both of A and R phases have a tetragonal crystal structure but B has an orthorhombic crystal system. The energy bandgaps of A-TiO₂, B-TiO₂ and, R-TiO₂ are 3, 3.31, 3 eV respectively. In addition to its bulk form, Titanium dioxide in the form of nanomaterials is utilized in many applications, for instance photocatalytic, gas sensor, pigments, and solid state solar cells [10-13]. The nanostructures of TiO₂ may be synthesized in the form of nanoparticles [14], nanorods, nanowalls [15], nanotubes [16], nanosheets [17] and nanofibers [18].

Despite the aforementioned features of TiO₂, there are some important flaws that limit their use in several applications, one of them is that the spectral region of maximum absorption in TiO₂ is located in the UV-region. Doping of TiO₂ with one of the transition metals such as; Co⁺³, Ni⁺², Fe³⁺, Cr³⁺, etc. is carried out to prevent or minimize the recombination processes and to drag its absorption-region into the visible-region [1,19]. It has been reported that doping TiO₂ with metallic ions can increase the absorption coefficient due to formation of additional energy states within the band gap of TiO₂.

The main roles which governs the right choice of TiO₂ for each application are the structure, morphology and the crystalline size of the TiO₂. These parameters could be determined by the method of preparation [8-9]. There are many techniques to prepare TiO₂ such as chemical vapor deposition [20], atomic layer deposition [21], DC Reactive Magnetron Sputtering [22], chemical path deposition [23], electrochemical anodization [24], spray pyrolysis deposition [25], Solvothermal [26], Ione-Assisted Electron-Beam Evaporation [27], Hydrothermal deposition (HD) [28] etc. Here we used the hydrothermal technique to fabricate TiO₂ films in nanorod structures.

2. Experimental Work

FTO substrates (F:SnO₂ from DyeSol company TEC 8 with 600 nm in thickness, dimensions 2×2 cm) were ultrasonically cleaned for 15 min with acetone, ethanol, and double-distilled water (DDW) (purchased from a local store) and then the substrates kept to dry in air, after that they were put at 45° tilt-angle along a wall of Teflon-liner in a homemade stainless steel autoclave as shown in Figure 1.

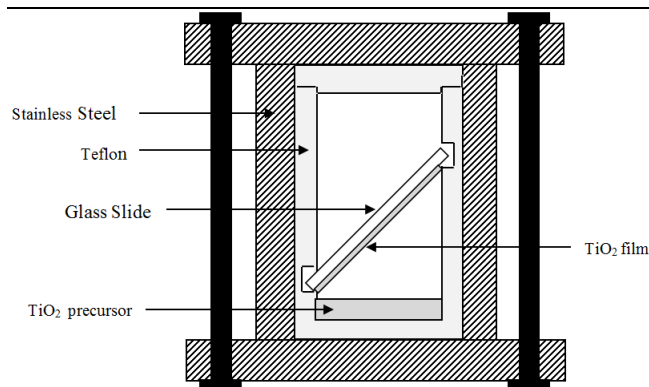


Figure 1. Illustrative diagram of the autoclave used to deposit TiO₂ nanorods films.

At first a volume of 20 ml of DDW was mixed with 20 ml of hydrochloric acid (concentrated 37%) using magnetic stirrer for 5min, the solution labeled is A1. After that, 1.017 ml and 1.033 ml of high purity of Titanium Butoxide as precursor of titanium oxide (purchased from Sigma Aldrich company, Germany) was mixed with A1 solution and then kept under stirrer for another 5 min. At this stage the solution is labeled A2. This is followed by adding Fe(NO₃)₃·9H₂O (HiMedia Laboratories Pvt. Ltd) as a precursor of Fe to A2 solution of ratios of Fe/Ti (0.1, 0.3, 0.7 and 1.5 at. %). The total solution is stirred again for 90 min. At first the mixture was white transparent but after adding the Iron nitrate-nonahydrate it become green and transparent. After 90 minutes, the mixture of volume 20 ml is charged to a stainless autoclave. The autoclave and the substrate were put in an electric oven which was already preheated at 180 °C (±3 ramp rate) for three hours. After that, the autoclave removed out of the oven and slowly cooled-down under stream of water and the FTO substrate brought out of the autoclave and rinsed with DDW many times to get rid of any extra reactants. Finally the samples were dried in air at room temperature for 15 min. The TiO₂ samples were characterized by XRD of Cu Kα (λ = 0.15406 nm) in the 2θ range 20 to 75° and step size 0.02°, (College of Education Ibn al-Haytham). The Field Emission Scanning Electron Microscope (FESEM) equipment supported with Energy Dispersive Spectroscopy (EDS) is used to investigate the morphology of the TiO₂ films in the nanoscale and the composition of the films, respectively. (Razi Applied Science Foundation-Tehran, Iran). U-Vis spectroscopy (Shimadzu UV-1900i in our Nanoscale laboratory) visible spectrophotometer in the range (370-1100 nm) at the room temperature, and diffuse reflectance spectroscope (DRS) (Avantes AvLight-DH-S-BAL Al-Nahrain University-Chemistry Department) are implemented to determine the optical properties of the TiO₂ films. PerkinEler LS55 spectrofluorometer equipped with 40 W Xenon lamp is used to obtain the photoluminescence (PL) spectrum. The detection wavelength range was in the range (325-1100 nm) and the laser excitation wavelength was 304 nm (Razi Applied Science Foundation-Tehran, Iran).

3. Results and Discussion

The XRD diffractogram for pure TiO₂ and 1.5%Fe doped TiO₂ nanorods are shown in figure 2. The peaks at 2θ = (35.946°, 62.673°, and 69.681°) are characteristic of the tetragonal rutile (R) TiO₂, and these are corresponding to the planes (101), (002) and (112), respectively. These peaks are agreeing well with those of (JCPDS 89-4920 card). Moreover, no another peak that related to A or B-TiO₂ or for Fe-atoms are observed. In Figure 2, we labeled the peaks of the FTO substrates by stars and the R-TiO₂ by the letter R. Similar results are reported by S. Manu et al. [29].

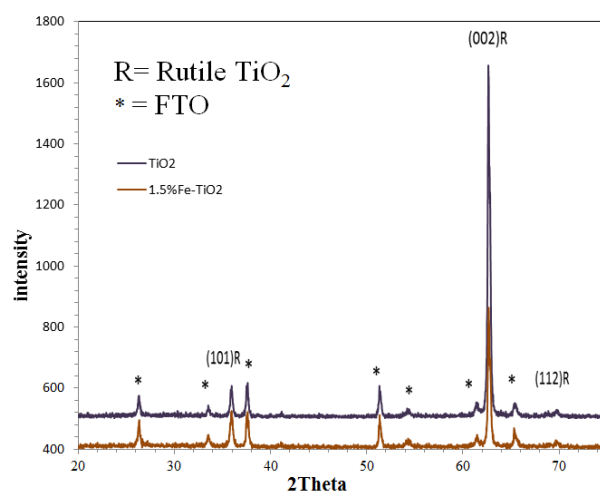
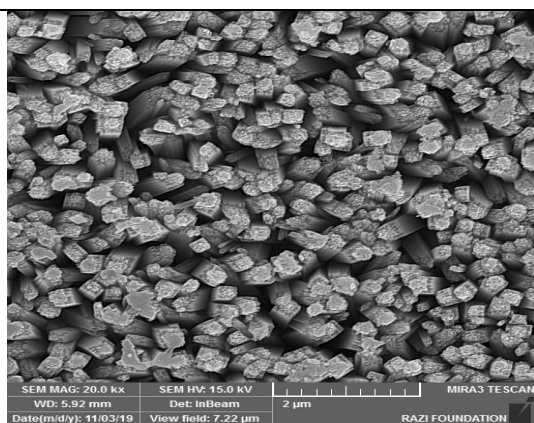
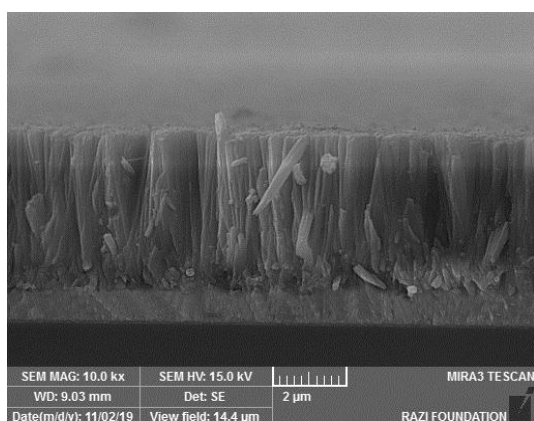


Figure 2. X-Ray diffractograms for the R-TiO₂ samples with pure and 1.5% Fe-doped TiO₂ deposited on the FTO-glass substrate by the hydrothermal method.

The FESEM images show that TiO₂ films deposited on the FTO substrate are vertically aligned nanorods and presented that there is no obvious effect of Fe doping on the vertical TiO₂ nanorods. The XRD analysis of Figure 3 confirmed the tetragonal structure of TiO₂ prepared by hydrothermal method and the doping has no marked effect on the crystalline structure of the R-TiO₂. The results agree with B. Liu et al. [28]. Top and cross-sectional views of TiO₂ nanorods are presented in Figure 3. The nanorods were grown vertically on the FTO substrate. It is clear from the figures that each nanorod had length larger than 4 μm and its cross-sectional area was square within 50-300 nm in diameter.



(a)



(b)

Figure 3. Pictures of FESEM of pure TiO₂ nanorods films prepared by hydrothermal technique (a) top-view (b) side-view.

The intrinsic defects and the extrinsic impurities can give arise to a specific properties of TiO₂, so that many researches worked on introducing extrinsic impurities into the TiO₂ structure to enhance the optical properties of the material. The absorption coefficient (α) spectrum is shown in Figure 4. α is calculated using Equation (1) below.

$$\alpha = 2.303 \frac{A}{t} \quad (1)$$

where A is the absorbance and t is the thickness of the films calculated from the FESEM measurements.

Figure 4 shows an explicit blue shift of the absorption coefficient. And by utilizing Equation (2) we can estimate the energy bandgap of the films by drawing $(\alpha h\nu)^2$ against $h\nu$ as shown in figure 5. The figure indicates that the bandgap of R-TiO₂ are of direct type. A similar direct bandgap of the undoped R-TiO₂ is also reported by C. Caoa et al. [30].

$$\alpha = \frac{A(h\nu - E_g)^n}{h\nu} \quad (2)$$

where A is a constant, h the universal Plank's constant, E_g the energy bandgap, ν the photon frequency. For direct transition n = 1/2.

We also note that the energy bandgap decreases slightly as the Fe dopant ratio is increased. The slight reduction in the bandgap is attributed to the fact that Fe atoms has enough energy to substitute titanium atoms in the TiO₂ lattice. This enhances transition of electrons from Fe-3d levels to the conduction band (CB) of TiO₂ [7]. This indicates a formation of intermediate states (tails) between the conduction and the valance bands since Ti and Fe are different in Electronegativity (1.54 for Ti) and (1.83 for Fe). These states increase in density with the increase in concentration Fe dopant. In figure 6 we have presented the calculated Urbach energy tails (E_u) which describe the width of the extended states underneath the conduction band.

The results illustrate that with the low Fe concentration (0.1%) the E_u decreased and then increase with increasing Fe content in TiO₂ as indicated in Table 1. The increment in E_u at higher concentration (1.5%) may be due to generation of more defects that introduced with increasing Fe dopant concentration.

Also we use the diffuse reflectance spectroscopy to calculate the energy bandgap from the reflectance spectra. In general, the results extracted from reflectance spectra agree well with those found from Uv-vis spectra as shown in Figure 7. However, the reflectance method gives energy gaps equal or greater than those calculated by UV-vis method. The results are introduced in Table 1.

Table 1. Energies band gap and Urbach of the samples by the UV-vis and Reflectance method.

Samples	E _g from UV-vis (eV)	E _g from reflectance (eV)	E _u (meV)
TiO ₂	3.12	3.25	630.28
0.1% Fe-TiO ₂	3.2	3.32	464.25
0.3% Fe-TiO ₂	3	3	640.82
0.5% Fe-TiO ₂	3.15	3.3	718.59
0.7% Fe-TiO ₂	3.15	3.36	1098.41
1.5% Fe-TiO ₂	3.0	3.28	1836.88

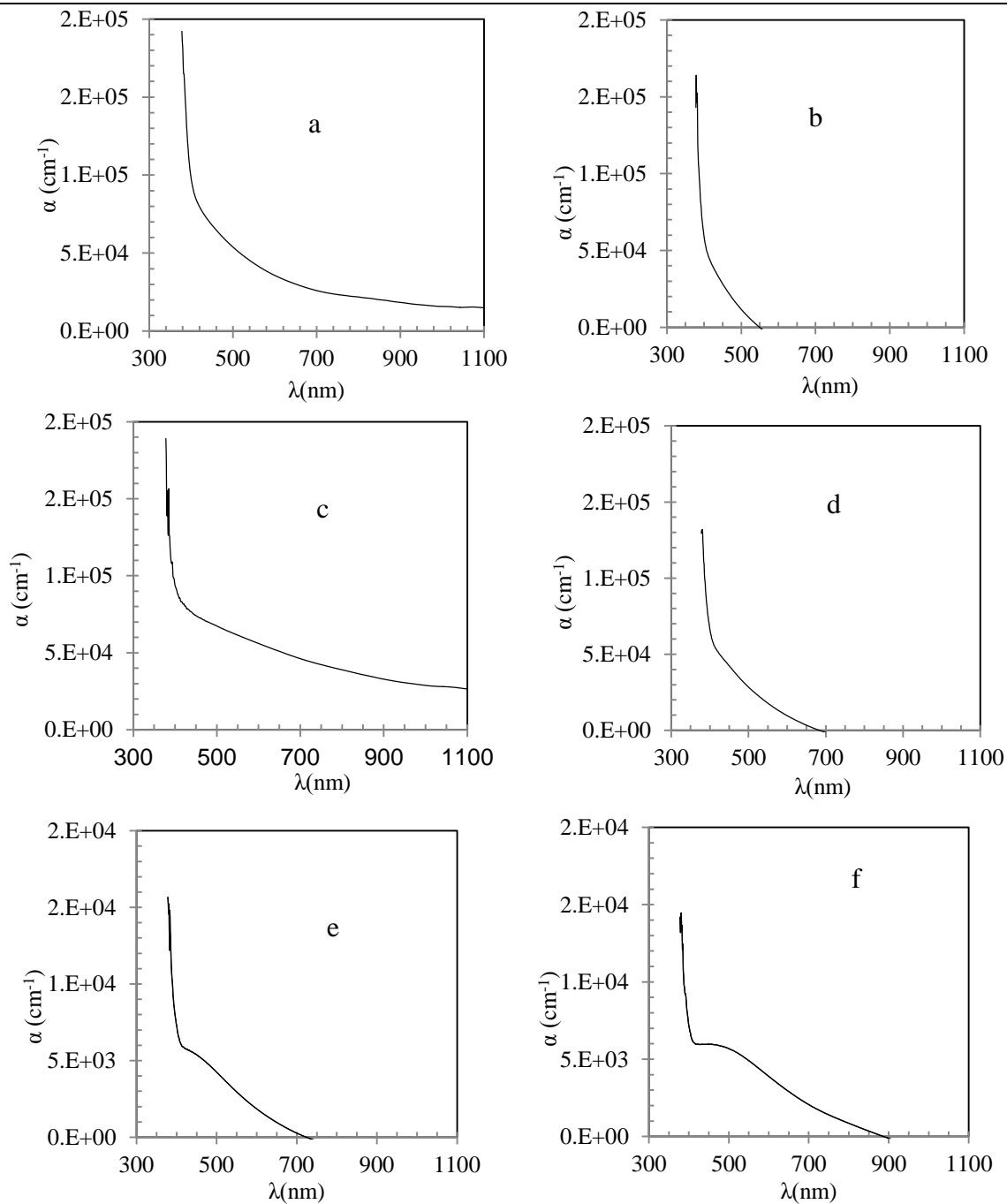


Figure 4. The Absorption coefficients of TiO_2 films prepared by Hydrothermal technique for the (a) TiO_2 , (b) TiO_2 -0.1%Fe(c) TiO_2 -0.3%Fe, (d) TiO_2 -0.5%Fe, (e) TiO_2 -0.7%Fe and (f) TiO_2 -1.5%Fe.

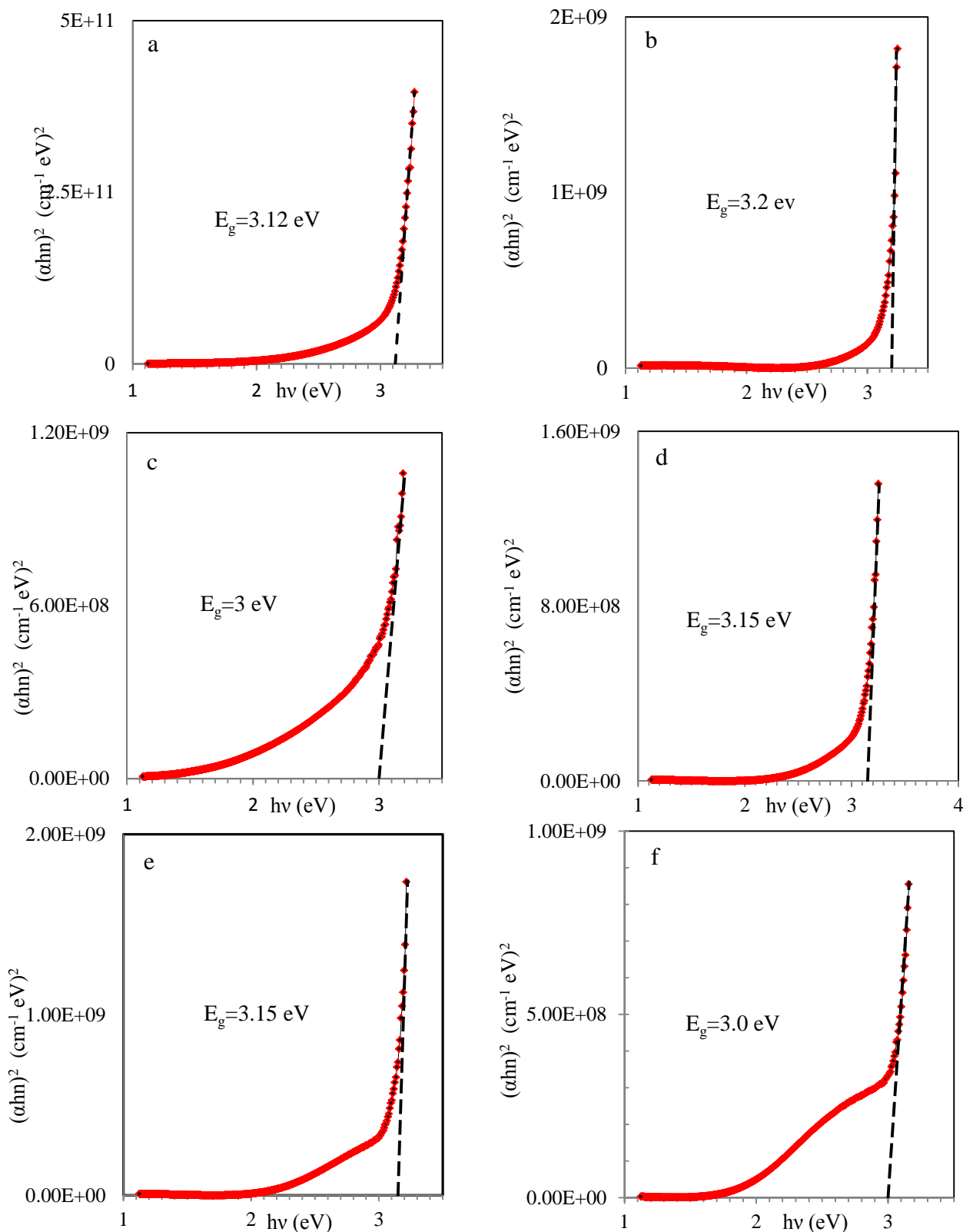


Figure 5. The energies bandgap of the samples(a) TiO_2 , (b) 0.1% Fe- TiO_2 , (c) 0.3% Fe- TiO_2 , (d) 0.5% Fe- TiO_2 , (e) 0.7% Fe- TiO_2 and (f) 1.5% Fe- TiO_2 from UV-visible measurements.

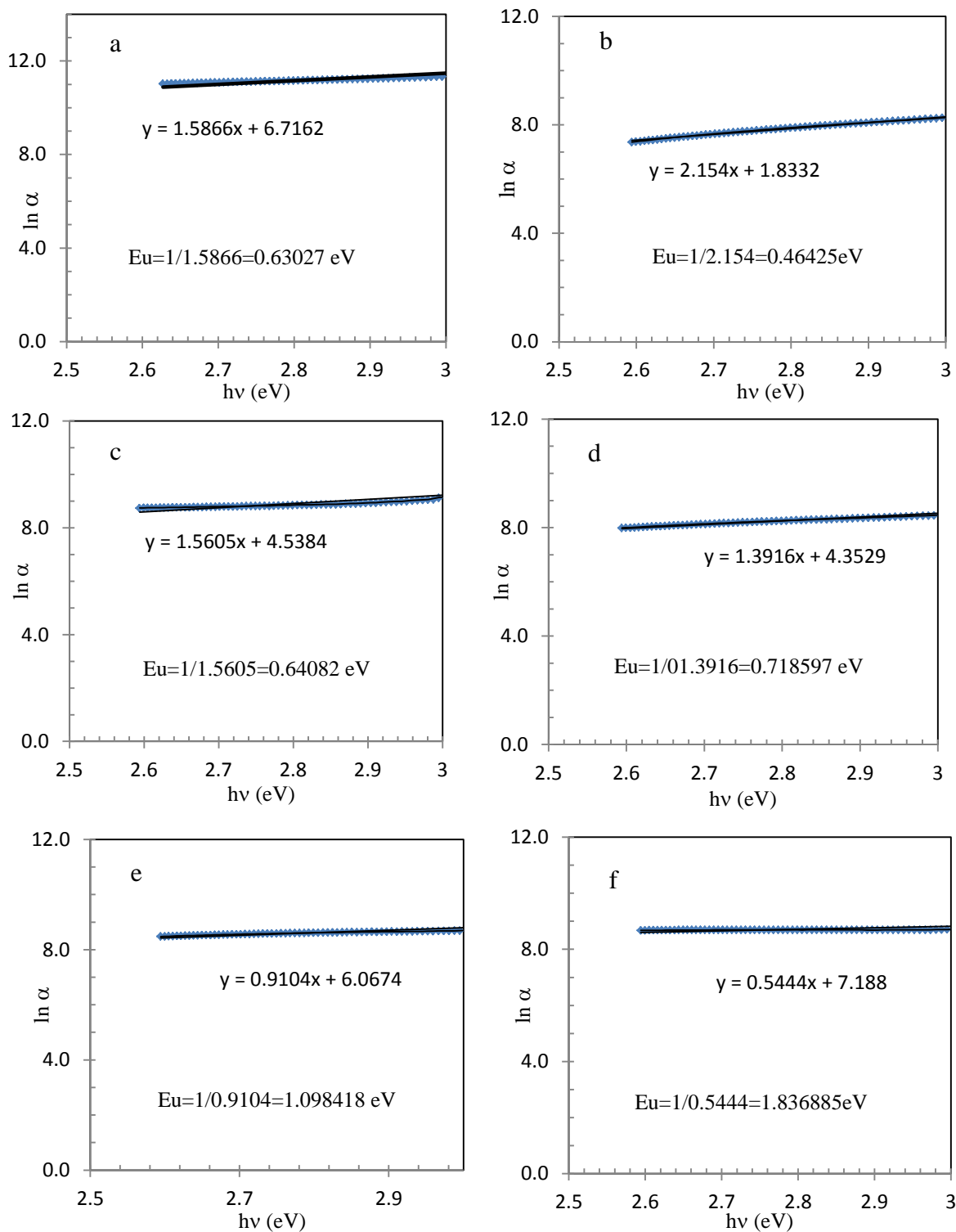


Figure 6. Urbach energy gap E_u for the samples (a) TiO_2 , (b) $\text{TiO}_2\text{-}0.1\%\text{Fe}$ (c) $\text{TiO}_2\text{-}0.3\%\text{Fe}$, (d) $\text{TiO}_2\text{-}0.5\%\text{Fe}$, (e) $\text{TiO}_2\text{-}0.7\%\text{Fe}$ and (f) $\text{TiO}_2\text{-}1.5\%\text{Fe}$.

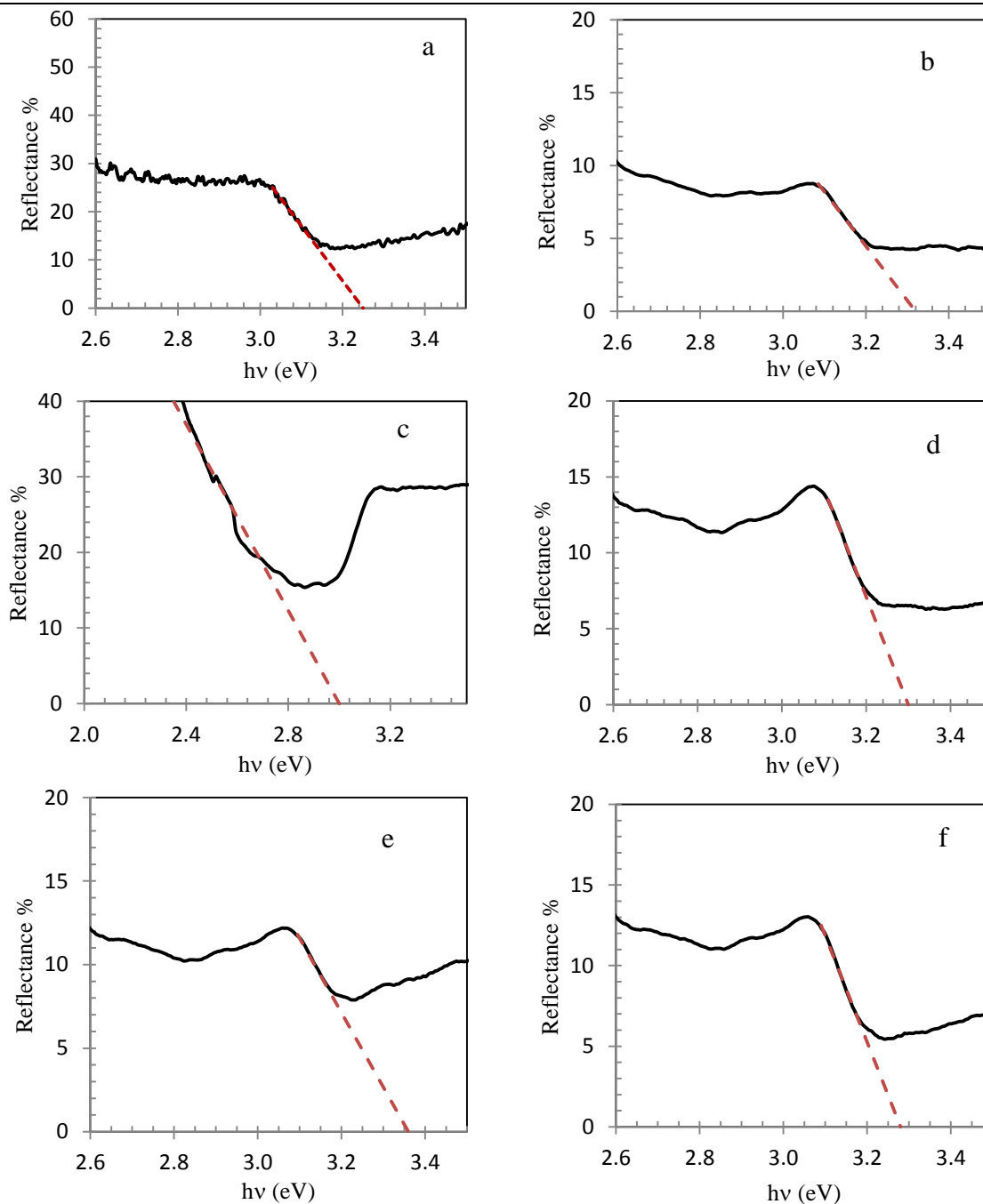


Figure 7. Reflectance of TiO_2 film prepared by Hydrothermal technique of the samples (a) TiO_2 , (b) TiO_2 -0.1%Fe(c) TiO_2 -0.3%Fe, (d) TiO_2 -0.5%Fe, (e) TiO_2 -0.7%Fe and (f) TiO_2 -1.5%Fe.

Figure 8 reveals the PL-spectra for undoped and Fe-doped TiO_2 films. The films are excited using wavelength 304 nm which corresponds to photon energy of 4.08 eV. The figures reveal sharp peaks at 607 nm and small peak at 909 nm. It was reported that the first emission is due to direct transitions from higher states in the conduction band to lower states in the valance band. The weak one may be caused by electrons trapped by the oxygen vacancies [31]. A similar sharp peak was reported by R. S. Ningthoujam et al. in Eu doped TiO_2 films [32]. Noticeably, there is no

broad emission band which belongs to the deep-level defects. As it can be seen from figures, the PL intensity at first decreases until it reaches its minimum value at Fe doping (0.1 at %), then increases as the Fe concentration increases. It is worthwhile to mention that at lower doping concentration, the recombination rate of electrons with holes is low. However, when ion concentration exceeds a certain limit it starts to aggregate and acts as recombination centers [33-35].

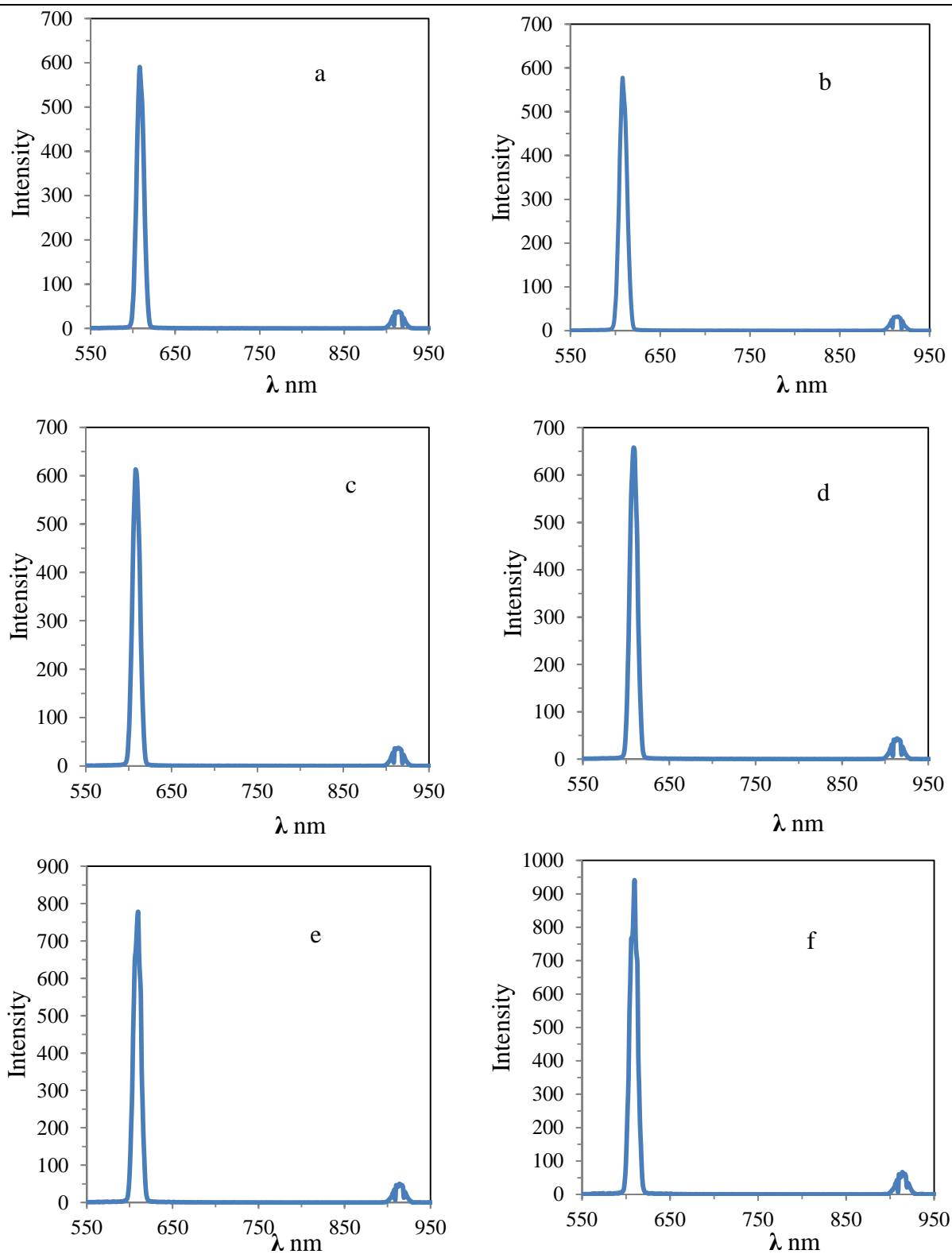


Figure 8. The PL spectra of (a) TiO₂, (b) TiO₂-0.1%Fe(c) TiO₂-0.3%Fe, (d) TiO₂-0.5%Fe, (e) TiO₂-0.7%Fe and (f) TiO₂-1.5%Fe.

4. Conclusions

In the present work, doping of titanium dioxide films with Fe-dopants has been implemented successfully using hydrothermal technique. The crystalline structure did not apparently changed with the doping process in the doping range (0.1-1.5 at %). The optical properties measurements revealed a slight reduction in the bandgap energy for the samples doped with high Fe concentration. Doping of TiO₂ with iron can be used actively and successfully to enhance its optical properties without deforming the crystallinity of the material.

5. References

- [1] Xie, Y.; Wei, L.; Wei, G.; Li, Q.; Wang, D.; Chen, Y.; Yan, S.; Liu, G.; Mei, L.; Jiao, J.; "A self-powered UV photodetector based on TiO₂ nanorod arrays"; *J. Nanoscale Research Letters*, 8:188, 2013.
- [2] Can, Z.; Wanyu, D.; Hualin, W.; Weiping, C.; Dongying, J.; "Influences of working pressure on properties for TiO₂ films deposited by DC pulse magnetron sputtering"; *J. Environmental Sciences* 21, 741-744, 2009.
- [3] Kim, C.; Kim, K. S.; Kim, H. Y.; Han, Y. S.; "Modification of a TiO₂ photoanode by using Cr-doped TiO₂ with an influence on the photovoltaic efficiency of a dye sensitized solar cell"; *J. Mater. Chem.* 18, 5809-5814, 2008.
- [4] Wisitsoraat, A.; Tuantranont, A.; Comini, E.; Sberveglieri, G.; Wlodarski, W.; "Characterization of n-type and p-type semiconductor gas sensors based on NiO_x doped TiO₂ thin films"; *J. Thin Solid Films* 517, 2775-2780, 2008.
- [5] Morsy, F. A.; El-Sherbiny, S.; Samir, M.; Fouad, O. A.; "Application of nanostructured titanium dioxide pigments in paper coating: a comparison between prepared and commercially available ones"; *Journal of Coatings Technology and Research* 13.2, 307-316, 2016.
- [6] Shifu, C.; Wei, L.; Sujuan, Z.; Yinghao, C.; "Preparation and activity evaluation of relative p-n junction photocatalyst Co-TiO₂/TiO₂"; *J. Sol-Gel Sci. Technol.* 54, 258-267, 2010.
- [7] Dholam, R.; Patel, N.; Adami, M.; Miotello, A.; "Hydrogen production by photocatalytic water-splitting using Cr- or Fe-doped TiO₂ composite thin films photocatalyst"; *J. Hydrogen energy* 34, 5337-5346, 2009.
- [8] Reyes-Coronado, D.; Rodríguez-Gattorno, G.; Espinosa-Pesqueira, M. E.; Cab, C.; de Coss, R. D.; Oskam, G.; "Phase-pure TiO₂ nanoparticles: anatase, brookite and rutile"; *J. Nanotechnology*, 19(14) 145605, 2008.
- [9] Mohammad A.; Behnajady, N.; Modirshahla, M.; Shokri, H.; Elham, H.; Zeininezhad, A.; "The effect of particle size and crystal structure of titanium dioxide nanoparticles on the photocatalytic properties"; *J. Environmental Science and Health Part A*, 43(5), 460-467, 2008.
- [10] Kim, C.; Kim, K. S.; Kim, H. Y.; Han, Y. S.; "Modification of a TiO₂ photoanode by using Cr-doped TiO₂ with an influence on the photovoltaic efficiency of a dye sensitized solar cell"; *J. Mater. Chem.* 18, 5809-5814, 2008.
- [11] Wisitsoraat, A.; Tuantranont, A.; Comini, E.; Sberveglieri, G.; Wlodarski, W.; "Characterization of n-type and p-type semiconductor gas sensors based on NiO_x doped TiO₂ thin films"; *Thin Solid Films* 517, 2775-2780, 2008.
- [12] Morsy, F. A.; El-Sherbiny, S.; Samir, M.; Fouad, O. A.; "Application of nanostructured titanium dioxide pigments in paper coating: a comparison between prepared and commercially available ones"; *J. Coat. Technol. and Res.* 13(2), 307-316, 2016.
- [13] Shifu, C.; Wei, L.; Sujuan, Z.; Yinghao, C.; "Preparation and activity evaluation of relative p-n junction photocatalyst Co-TiO₂/TiO₂"; *J. Sol-Gel Sci. Technol.* 54, 258-267, 2010.
- [14] Viana, M.M.; Soares, V. F.; Mohallem, N. D. S.; "Synthesis and characterization of TiO₂ nanoparticles"; *J. Ceramics International* 36, 2047-2053, 2010.
- [15] Wu, J. J.; Yu, C. C.; "Aligned TiO₂ Nanorods and Nanowalls"; *J. Phys. Chem. B*, 108(11), 3377-3379, 2004.
- [16] Jun, Y.; Parkwb, J. H.; Kang, M. G.; "The preparation of highly ordered TiO₂ nanotube arrays by an anodization method and their applications"; *J. Chem. Commun.* 48, 6456-6471, 2012.
- [17] Chen, J. Song and Lou, D. X. Wen. "Anatase TiO₂ nanosheet: An ideal host structure for fast and efficient lithium insertion/extraction"; *J. Electrochemistry communications*, 11(12), 2332-2335, 2009.
- [18] I-Doo Kim; Rothschild, A.; Hong Lee, B.; Young Kim, D.; Mu Jo, S.; Tuller, H. L.; "Ultrasensitive Chemiresistors Based on Electrospun TiO₂ Nanofibers"; *J. Nano Lett.*, 6(9), 2009-2013, 2006.
- [19] Wan, L.; Gao, Y.; Xia, X. H.; Deng, Q. R.; Shao, G.; "Phase selection and visible light photo-catalytic activity of Fe-doped TiO₂ prepared by the hydrothermal method"; *Materials Research Bulletin*, 46(3), 442-446, 2011.
- [20] Yeung, K. S.; Lam, Y. W.; "A Simple Chemical Vapor Deposition Method for Depositing Thin TiO₂ Films"; *J. Thin Solid Films*, 109, 169-178, 1983.
- [21] Shin, H.; Jeong, D.; Lee, j.; Sung, M. M.; Kim, J.; "Formation of TiO₂ and ZrO₂ Nanotubes Using Atomic Layer Deposition with Ultraprecise Control of Wall Thickness." *J. Advanced Materials*, 14, 1197-1200, 2004.
- [22] Lindgren, T.; Mwabora, J. M.; Avendan, E.; Jonsson, J.; Hoel, A.; Granqvist, C. G.; Lindquist, S. E.; "Photoelectrochemical and Optical Properties of

- Nitrogen Doped Titanium Dioxide Films Prepared by Reactive DC Magnetron Sputtering”; *J. Phys. Chem. B*, 107, 5709-5716, 2003.
- [23] Mayabadia, A.H.; Wamana, V. S.; Kamblea, M.M.; Ghosha, S. S.; Gabhalea, B. B.; Rondiya, S.R.; Rokadea, A. V.; Khadtarea, S. S.; Sathe, V. G.; Pathan, H. M.; Gosavic, S.W.; Jadhav, S. R.; “Evolution of structural and optical properties of rutile TiO₂ thin films synthesized at room temperature by chemical bath deposition method”; *J. Physics and Chemistry of Solids*, 75, 182-187, 2014.
- [24] Wang, J.; Lin, Z.; “Freestanding TiO₂ Nanotube Arrays with Ultrahigh Aspect Ratio via Electrochemical Anodization”; *J. Chem. Mater.*, 20, 1257-1261, 2008.
- [25] Okuya, M.; Nakade, K.; Kaneko, S.; “Porous TiO₂ thin films synthesized by a spray pyrolysis deposition (SPD) technique and their application to dye-sensitized solar cells”; *J. Solar Energy Materials & Solar Cells*, 70, 425-435, 2002.
- [26] Yang, G.; Jiang, Z.; Shi, H.; Jones, M. O.; Xiao, T.; Edwards, P. P.; Yan, Z.; “Study on the Photocatalysis of F-S co-doped TiO₂ Prepared Using Solvothermal Method”; *J. Applied Catalysis B: Environmental*, 96, 458-465, 2010.
- [27] Bhattacharyya, D.; Sahoo, N.K.; Thakur, S.; Das, N.C.; “Spectroscopic Ellipsometry of TiO₂ Layers Prepared by Ion-Assisted Electron-Beam Evaporation”; *J. Thin Solid Films*, 360, 96-102, 2000.
- [28] Liu, B.; Aydil, E. S. “Growth of Oriented Single-Crystalline Rutile TiO₂ Nanorods on Transparent Conducting Substrates for Dye-Sensitized Solar Cells”; *J. Am. Chem. Soc.* 131, 3985–3990, 2009.
- [29] Manu, S.; Abdul Khader, M.; “Non-uniform distribution of dopant iron ions in TiO₂ nanocrystals probed by X-ray diffraction, Raman scattering, photoluminescence and photocatalysis”; *J. Mater. Chem. C* 3, 1846-1853, 2015.
- [30] Cao, C.; Hu, C.; Wang, X.; Wang, S.; Tian, Y.; Zhang, H.; “UV sensor based on TiO₂ nanorod arrays on FTO thin film”; *J. Sensors and Actuators B* 156, 114-119, 2011.
- [31] Mali, S. S.; Shinde, P. S.; Betty, C. A.; Bhosale, P. N.; Lee, W. J.; Patil, P. S. “Nanocoral architecture of TiO₂ by hydrothermal process: synthesis and characterization”; *J. Applied Surface Science*, 257(23), 9737-9746, 2011.
- [32] Ningthoujam, R. S.; Sudarsan, V.; Vatsa, R. K.; Kadam, R. M.; Gupta, A. “Photoluminescence studies on Eu doped TiO₂ nanoparticles”; *J. Alloys and Compounds*, 486(1-2), 864-870, 2009.
- [33] Li, F. B.; Li, X. Z.; Ao, C. H.; Lee, S. C.; Hou, M. F. “Enhanced photocatalytic degradation of VOCs using Ln³⁺-TiO₂ catalysts for indoor air purification”; *J. Chemosphere*, 59(6), 787-800, 2005.
- [34] Choi, W.; Termin, A.; Hoffmann, M. R. “The role of metal ion dopants in quantum-sized TiO₂: correlation between photoreactivity and charge carrier recombination dynamics”; *J. Physical Chemistry*, 98(51), 13669-13679, 2002.
- [35] Liqiang, J.; Yichun, Q.; Baiqi, W.; Shudan, L.; Baojiang, J.; Libin, Y.; Jiazhong, S. “Review of photoluminescence performance of nano-sized semiconductor materials and its relationships with photocatalytic activity”; *J. Solar Energy Materials and Solar Cells*, 90(12), 1773-1787, 2006.